Supporting Information for
Digital actuation control of soft robotic origami with self-folding liquid crystal elastomer hinges

David C. Bershadsky[1], Tuo Zhao[2], Glaucio H. Paulino[2,3*], Emily C. Davidson[4*],
[*]Corresponding authors. Email: gpaulino@princeton.edu, edavidson@princeton.edu

This PDF file includes:

Other Supporting Information for this manuscript:

Data S1. Princeton Data Commons:
`https://datacommons.princeton.edu/discovery/catalog/doi-10-34770-q55n-0m58`

S1: Thermal Analysis of Localized Joule Heating

The power delivered under Joule heating (heating rate) is a direct function of the current and voltage. Power is defined as $P = IV = I^2R$. Since we are using a constant current driver with constant voltage, both I and V are constant. Power regulation is then achieved using pulse width modulation (PWM) control, where a duty cycle is defined as the fraction of the pulse period when the output is turned on. The power output is then defined as $P = IV \times dutycycle\%$. The heating and cooling profiles are characterized in Fig. S1, showing the localization of the Joule heating as well as the thermal diffusion during the subsequent cooling cycles.

The integrated Joule heater flex-PCBs were designed with integrated copper 'dead zones' included in the unused areas between hinges. These copper zones serve a dual purpose. The first is to act as heat dissipation devices, enabling heat transport away from the LCE hinge to a larger surface area for faster cooling. The second, due to the rapid cooling experienced in these large surface area regions, they enhance thermal isolation between nearby hinges, minimizing their impact on each other. Fig. S1A-D illustrate these thermal effects via temperature profiles and thermal imaging. Fig. S1A shows the thermal profile during a heating cycle, exhibiting a tall and narrow peak around the LCE hinge. Fig. S1B-C show a cooling cycle with lower, but slightly wider peaks. The three thermal profiles are compared in Fig. S1D, illustrating their relative height and widths. The thermal conductance of copper is 385.0 W/mK and the copper used in the PCB heater coils uses $\sim$ 11.6 µm thick traces. The serpentine geometry of the heater results in the heater being separated from the copper cooling pads by $\sim$ half the width of the hinge with only a $\sim$ 2 mm wide region connecting it. As a result, neighboring hinges are minimally impacted during heating. During cooling, the heat transports slowly through the LCE, leading to sharp local thermal gradients; it is then rapidly conducted by the copper cooling pads, resulting in a sharp drop-off in temperature, as shown in Fig. S1(A). Depending on the thermal saturation of local cooling pads, the width of the peak expands, as shown by Cooling Profile 2 (Fig. S1(B-C)).

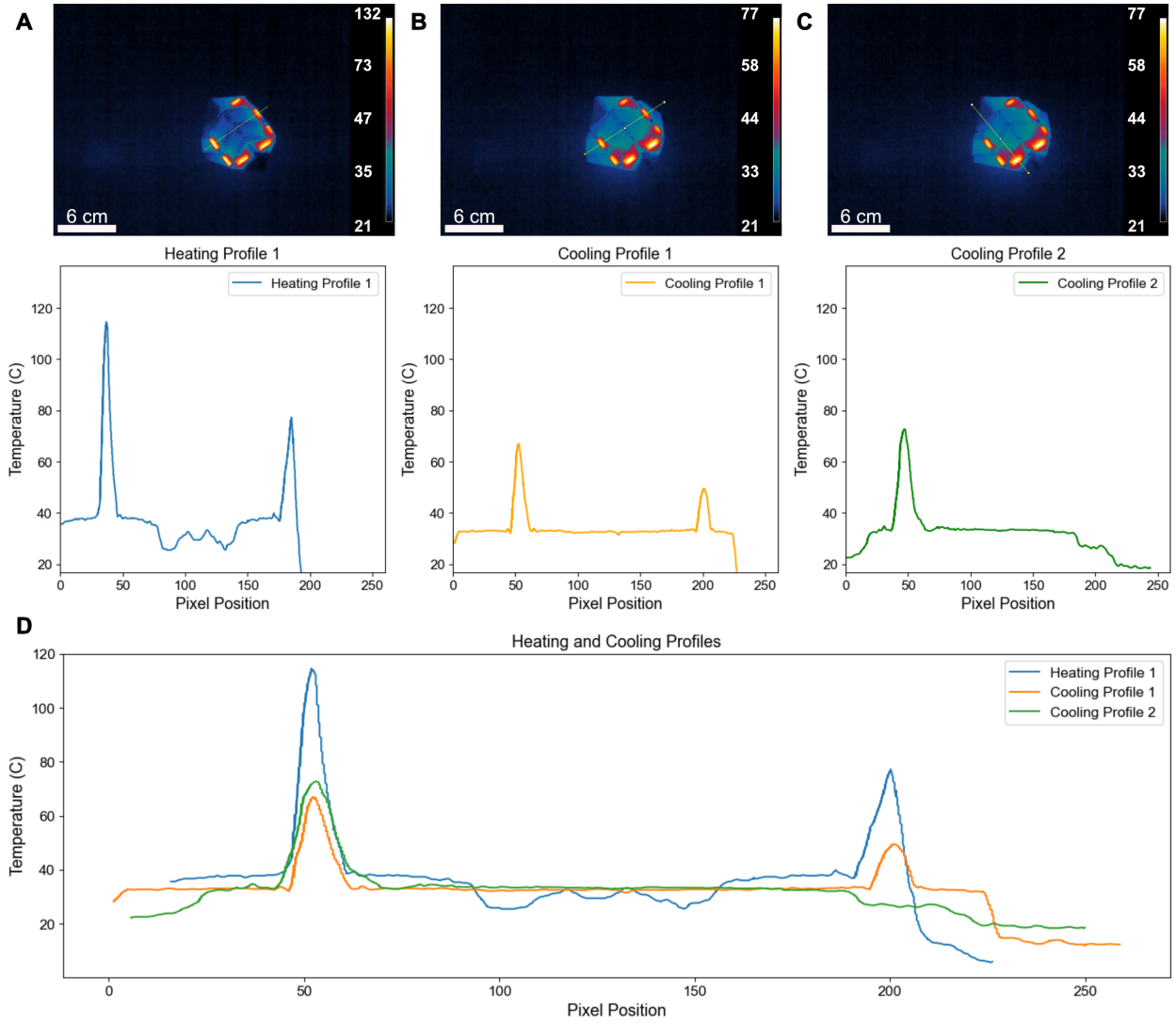

Figure S1: **Thermal Analysis of Localized Joule Heating.** This figure depicts thermal profiles along 3 excerpts of thermal imaging at two time points. (A) Shows the profile of temperature across the entire structure, spanning 6 visible hinges at peak power output and temperature (132°C), showing very narrow isolated thermal peaks. (B-C) Show two profiles of the same time point. The depicted traces show narrow isolated peaks with little to no heating of neighboring hinges. (D) depicts all three profiles overlaid such that the width of each hinge peak can be compared.

S2: Repeatability, Durability, and Long-Term Stability of LCE Actuation

Repeatability, durability, and long-term stability of the LCE hinges were formally characterized during cyclic actuation testing at various duty cycles as well as informally during imaging of additional samples. During duty cycle testing, each tested sample was cycled at least six times at each duty cycle (1%, 2%, and 3%) in both loaded (2 g) and unloaded configurations for a total of at least 36 cycles for this test. Within these thirty-six cycles, no noticeable degradation was observed. Additional cyclic testing was performed using the PID controller and a step response function. Greater than 1500 sequential cycles were performed with no noticeable degradation or delamination after some initial cycles (Fig. 5).

Durability of the LCE hinges is expected to be limited by two factors: thermal degradation of the Flex-PCB substrate and delamination of the LCE hinge from the structural Flex-PCB elements. To mitigate these factors, the Flex-PCB material was selected for its ability to withstand sustained heating up to 200 °C with short exposure up to 400 °C. These temperatures are far beyond the designed operating range of our hinges ($t \leq 120$ °C).

Delamination from the heating element is not a major concern due to the heating element being fully encapsulated by the LCE. As a result of this, if delamination occurs, the heating element will still be contained and maintain good contact and thus thermal transfer to the hinge. Delamination along the edge of the hinge does, however, pose a significant concern. Adhesion between the printed LCE and Kapton substrate used in the Flex-PCBs is poor due to the extremely smooth nature of the Kapton surface (Fig. S2A). To prevent delamination, a large overlap region was maintained between the Flex-PCB and the LCE, allowing encapsulation along three sides. Additionally, the FR4 stiffener panels, composed of a fire-retardant epoxy-impregnated fiberglass material, have a rough surface texture, facilitating mechanical LCE adhesion and improving hinge durability. A close-up of the hinge edge area is shown in Fig. S2B.

Long term stability of LCE actuation was tested by actuating LCE hinges up to 1.5 year post fabrication. Samples that had been previously cycled showed no noticeable degradation in bending performance.

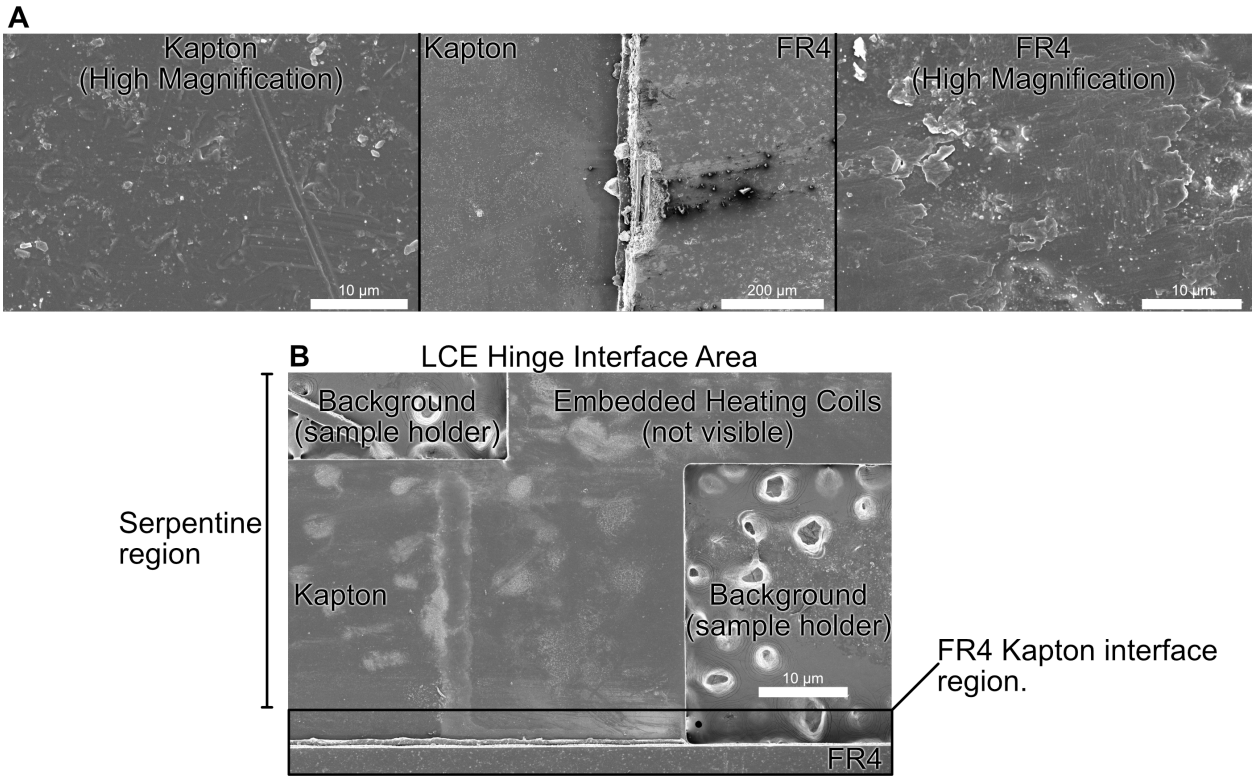

Figure S2: **Substrate Surface SEM.** (A) SEM images of Kapton and FR4 substrate materials shown in high magnification, along with a wider image of a Kapton-FR4 interface area on the Flex-PCB substrate. (B) SEM of a small segment of the hinge substrate region.

S3: Statistical Methods

The methods used in analyzing the data included in this work are detailed in this section. Full datasets, raw data, and full data processing scripts are included in the Princeton Data Commons repository linked in section Data S1. The bending and torque data in Fig. 2B-C were collected at fixed temperature intervals in a temperature controlled environment. Bending data was collected for at least three replicates for each sample. The data from each replicate is interpolated onto a common temperature axis in order to allow for averaging of data points. The associated error bars are given as the standard deviation of the sample average. In Fig. 2C, to estimate the applied gravitational torque during loaded bending tests, we model the load as a point mass m acting at a fixed moment arm d from the hinge. The gravitational force magnitude is $F_g = m \times g$, where g is the gravitational acceleration. The torque magnitude about the hinge is

$$\tau = \|\mathbf{r} \times \mathbf{F}\| = r F_g \sin\phi, \tag{S1}$$

where $\mathbf{r}$ is the position vector from the hinge to the load attachment point, $r = \|\mathbf{r}\| = d$, and ϕ is the included angle between $\mathbf{r}$ and the force direction.

In our geometry, the bending angle change $\Delta\theta(T)$ (reported in degrees) determines the orientation of the moment arm relative to gravity. Defining $\phi(T) = \Delta\theta(T)$, Eq. (S1) becomes

$$\tau(T) = mgd \sin\big(\phi(T)\big) = mgd \sin\big(\Delta\theta(T)\big). \tag{S2}$$

The duty cycle actuation data pictured in Fig. 4 and supplemented in Fig. S6, show representative traces for each data point. Due to the presence of a high frequency noise artifact created by the motion capture technique, a low pass Butterworth filter has been applied to the data. Fig. 5 does not use this filtering due to higher quality recording.

The data shown in Fig. S8 contains averaged and interpolated data across six LCE samples. Again, due to several repeated experiments, the data were interpolated to a common temperature axis. The error bars represent the standard deviation of the measurements.

The data shown in Fig. S1 is the extracted intensity of each pixel along the line drawn on each image rescaled to the min and max temperatures measured in that image.

S4: OriCadLCE Usage Overview

OriCadLCE is a complete computer-aided design (CAD) program designed to simplify the design and manufacturing of self-folding origami via LBL-DIW LCE printing. The program relies on 2D sketches using primitive geometries to define structural elements, folds, stiffeners, adhesives, and other elements, similar to popular CAD programs like Fusion 360. OriCadLCE has a layer management system, similar to those found in photo-manipulation tools like Photoshop, allowing the user to design multi-layer origami structures with interlocking elements, which can be printed using the LBL-DIW fabrication process. The select primitive menu (Fig. S3-1) allows the user to draw a number of primitive geometries. The Fold Type menu (Fig. S3-2) operates similarly, allowing the user to define an origami fold. The red Mountain Fold button (Fig. S3-3) toggles between mountain and valley folds. Similarly the 'Stiff Top' and 'Adhesive Top' buttons toggle whether stiffeners or adhesives are being placed on the top or bottom of the current layer (Fig. S3-4-5). The dynamic fold width button allows the user to toggle between setting a custom width

for each fold or setting a fixed width for all new folds (Fig. S3-6). The add stiffener and add adhesive buttons allow the user to define a polygon object to demarcate modifier regions (Fig. S3-7-8). The right panel controls both the background grid view and layer management (Fig. S3-9). The user can add/subtract layers, manage visibility, and select the active editing layer. The pan button toggles a panning mode, allowing the user to navigate around the workspace (Fig. S3-10). Inspection mode allows the user to edit elements that have already been placed, modifying parameters and deleting objects (Fig. S3-11). The snap buttons control the snap to grid, toggling on and off as well as changing the snap size (Fig. S3-12-13). The zoom and reset buttons allow the user to navigate the workspace and find their way home if they get lost (Fig. S3-14-16). Buttons 17-21 (Fig. S3-17-21) allow undo/redo functionality as well as saving, loading, and opening new files. Many of these buttons are mapped to their traditional keyboard shortcuts. The 'checkfold' button resolves mechanical conflicts between folds (Fig. S3-22). The export button (Fig. S3-23) displays the export panel where the user can input all relevant fabrication parameters. The lower half of (Fig. S3) shows a typical OriCadLCE design workflow.

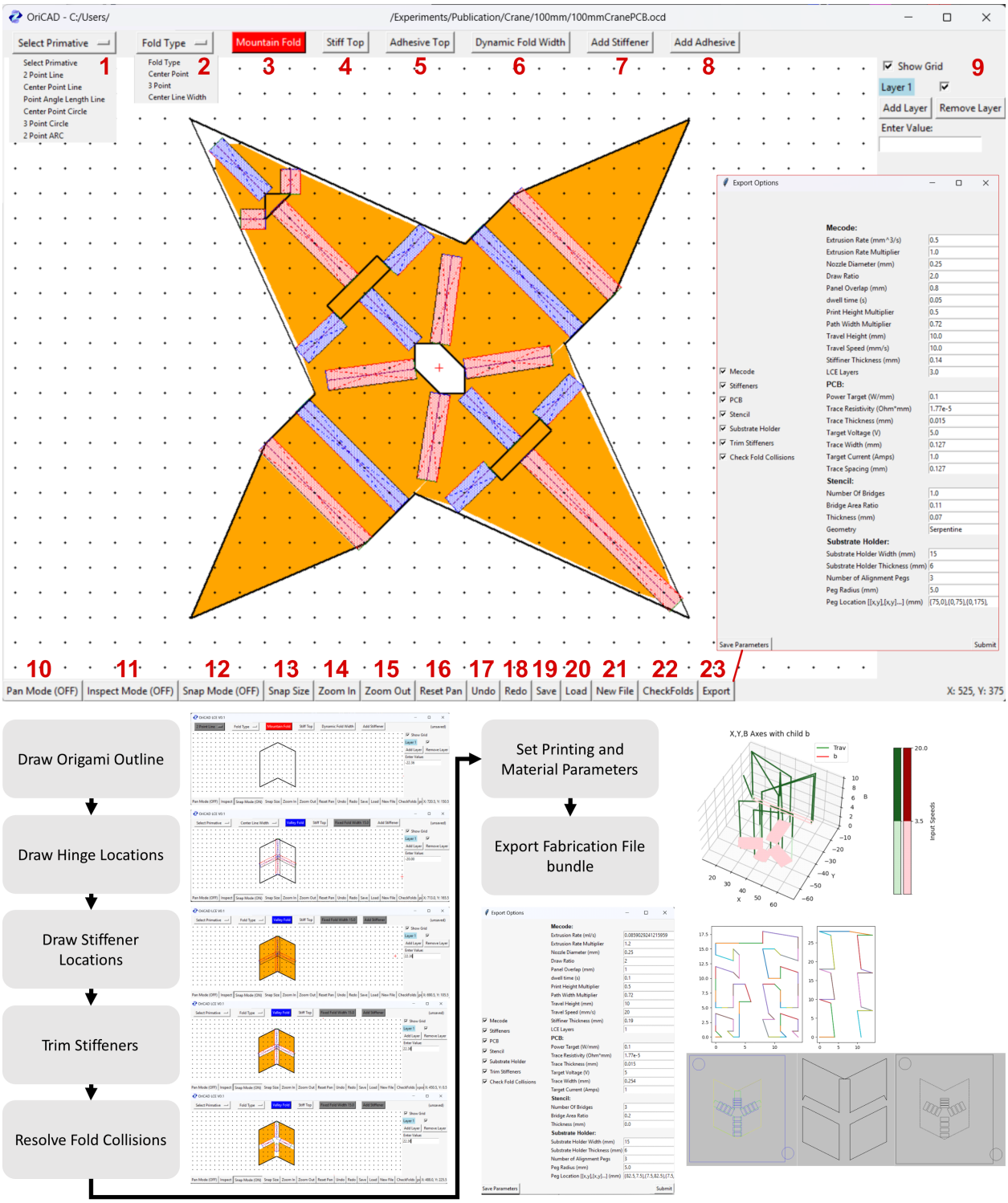

Figure S3: **OriCADLCE User Interface.** The OriCadLCE GUI is displayed with a typical design workflow illustrated below.

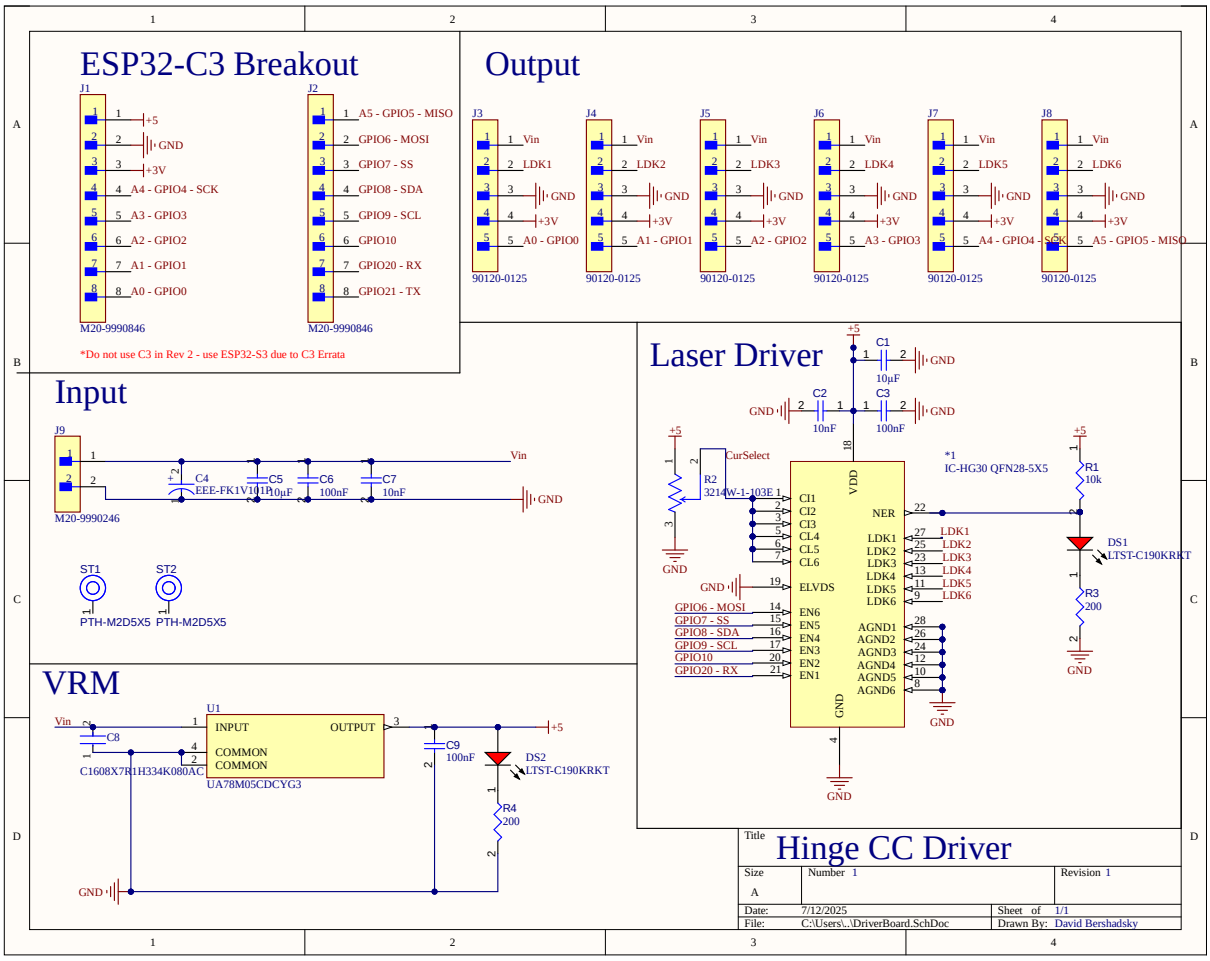

Figure S4: **PCB Driver Schematics.** The schematics of the constant current Joule hinge driver are detailed above.

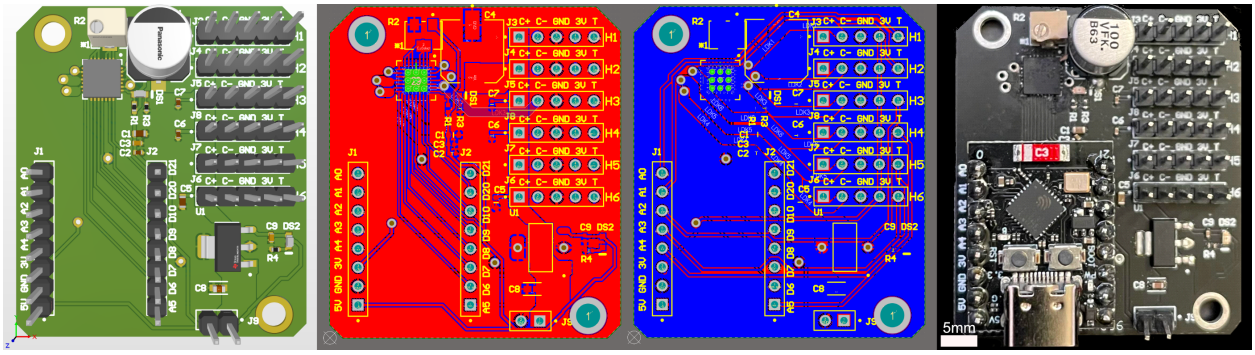

Figure S5: **PCB Driver Design.** The PCB layout, including 3D render, top and bottom layers, and final PCB, is shown. Due to issues with the ESP32-C3 detailed in the ESP32-C3 errata, we recommend using the ESP32-S3 as a drop-in replacement for the C3.

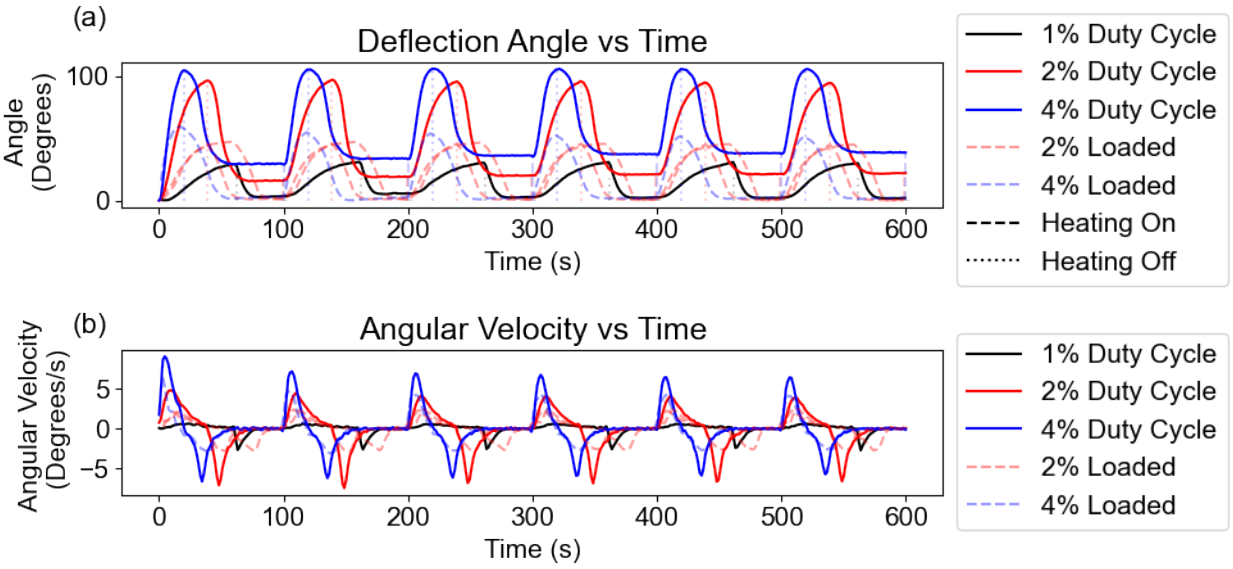

Figure S6: **Loaded hinge Actuation Performance.** Performance under a 2 g is overlaid on top of the unloaded actuation for (1%, 2%, and 4%) duty cycles. (A) depicts bending angle as a function of time. (B) Illustrates angular velocity over time. Due to a data collection error, the 1% duty cycle is not shown under load; the 2% duty cycle is instead shown a second time, but following the 1% cycle timings.

S5: Actuation Performance Under Load

Actuation torque and steady-state bending angle depend on hinge temperature through the LCE thermomechanical response. Accordingly, under an applied load, we expect reduced steady-state bending angles and lower peak angular velocities relative to the unloaded case. Loaded actuation data for the Flex-PCB hinge at each of the three tested duty cycles are shown in Fig. S6. Under a 2 g load, the response is consistent with a gravitationally imposed torque given by $\tau = mgd\sin(\Delta\theta)$, with temperature-dependent bending angles. Unloaded bending angle and equilibrium torque as functions of temperature are shown in Fig. 2B-C, and the measured torque magnitudes are comparable to prior LCE actuator reports (*26*).

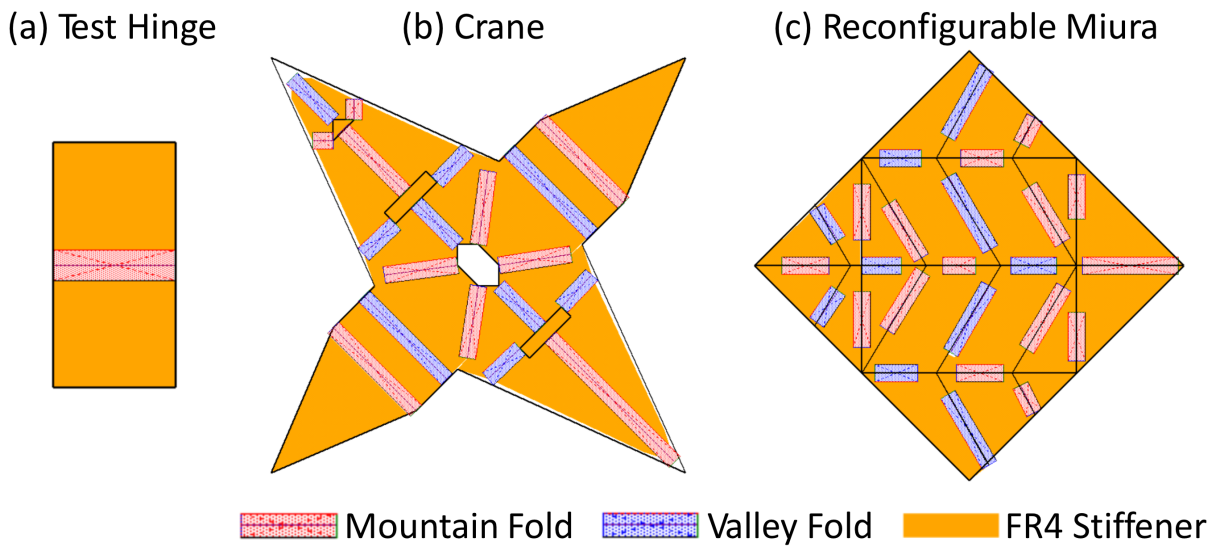

Figure S7: **Origami Fold Patterns.** The origami fold patterns used in this work are illustrated. (a) is the test hinge design used for all characterization work. The crane is detailed in (b) and the Miura sheet is shown in (c).

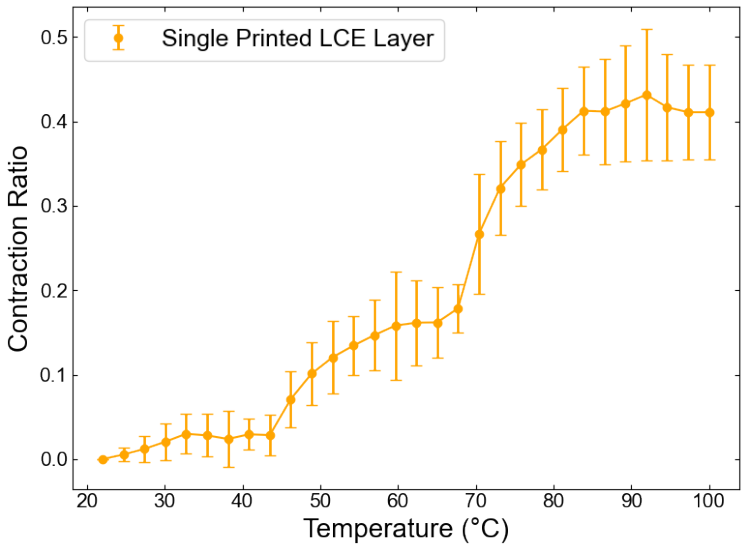

Figure S8: **LCE Contraction.** (A) Single-layer sheets of printed LCE were heated in an oil bath to verify contraction performance from 22 °C to 100 °C. Contraction ratio is defined as: $1 - \frac{\text{Current Length}}{\text{Initial Length}}$ Approximately 42% contraction is observed over the temperature range.

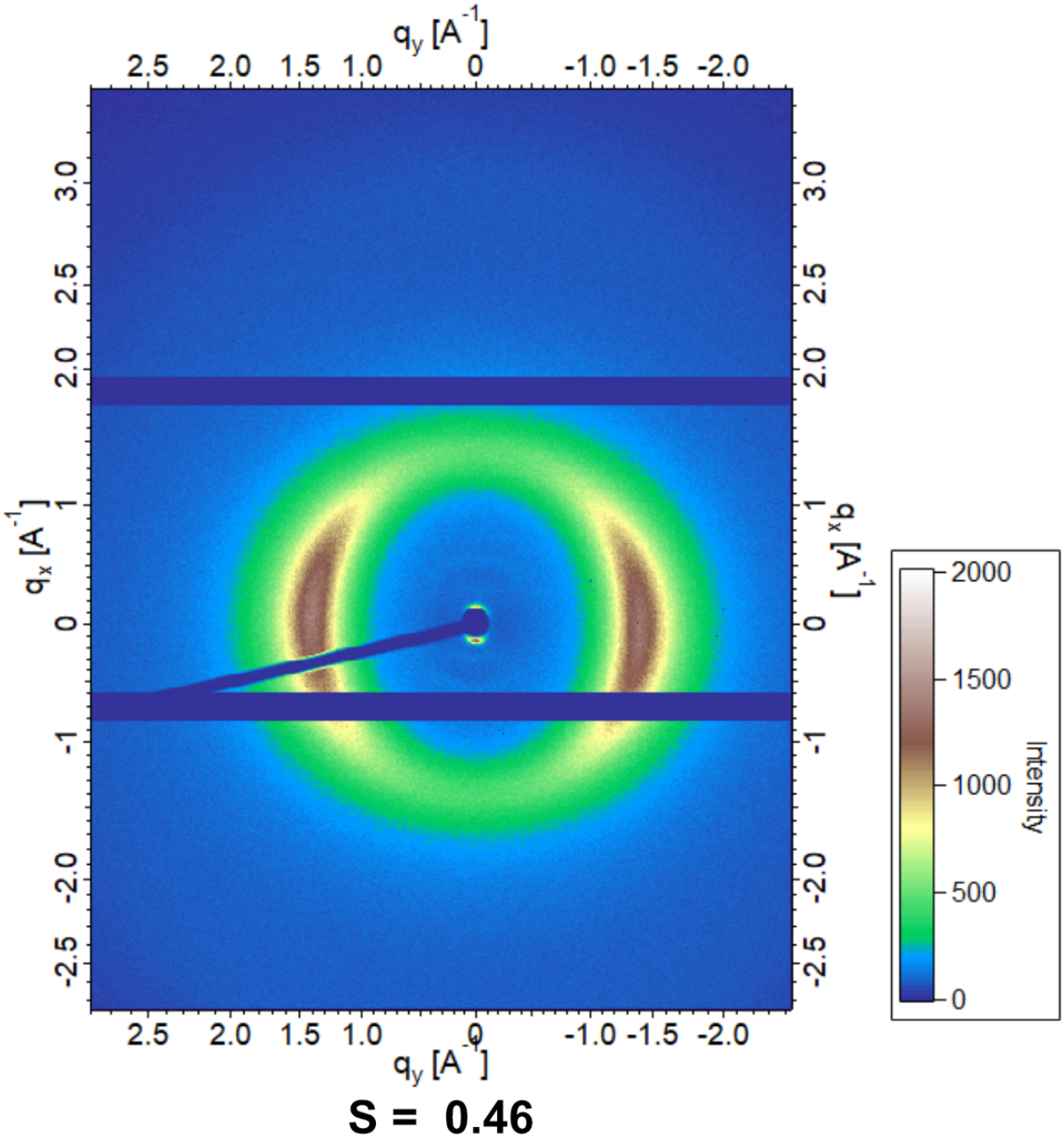

Figure S9: **LCE Alignment.** A wide-angle X-ray scattering (WAXS) (transmission) pattern of a three-layer uniformly aligned LCE sample with calculated scalar order parameter S = 0.46.

Table S1: **Flex-PCB Fabrication Parameters** The fabrication parameters used for the Flex-PCB substrates are detailed in this table.

Parameter	Value
Substrate Type	25 μm dielectric thickness
Layers	2
Product Type	Industrial/Consumer electronics
Different Design	1
Delivery Format	Single PCB
PCB Thickness	0.11 mm
Specify Stackup	no
Coverlay Color	Yellow
Silkscreen	White
Copper Type	Electro-deposited
Surface Finish	ENIG
Gold Thickness	1U"
Outer Copper Weight	1/3 oz
Coverlay Thickness	PI:12.5 μm/AD:15 μm
Gold Fingers	No
Stiffener	FR4
EMI Shielding Film	Without
Cutting Method	Laser Cutting
FR4 Thickness	0.1 mm
Electrical Test	Flying Probe Fully Test
Mark on PCB	Order Number
Silkscreen on Stiffener	No
Appearance Quality	IPC Class 2 Standard
Paper between PCBs	No
Outline Tolerance	±0.1 mm

Table S2: **LCE Ink Formulation.** All components used in the LCE ink are listed by CAS number, supplier, and quantity for a 6.5 g batch.

Chemical	**CAS No.**	**Supplier**	**Quantity**
RM82/C6M (Liquid Crystal Mesogen)	125248-71-7	Wilshire Technologies	5 g
(Ethylenedioxy)diethanethiol (EDDT)	14970-87-7	Sigma-Aldrich	1.331 mL
Butylated hydroxytoluene (BHT)	128-37-0	Acros	0.1298 mg
Dimethylolpropionic acid (DMPA)	4767-03-7	Acros	0.0974 g
Triallyl triazine trione (TATATO)	1025-15-6	Sigma-Aldrich	0.1071 mL
Triethanolamine (TEA)	102-71-6	Sigma-Aldrich	0.0894 mL

Table S3: **LCE Printing Parameters** The printing settings used in OriCadLCE are detailed in this table.

Parameter	Value
Extrusion Rate (mm^3/s)	0.5
Extrusion Rate Multiplier	1.0
Nozzle Diameter (mm)	0.25
Draw Ratio	2.0
Panel Overlap (mm)	0.8
Dwell Time (s)	0.05
Print Height Multiplier	0.5
Path Width Multiplier	0.72
Travel Height (mm)	10
Travel Speed (mm/s)	10
Stiffener Thickness (mm)	0.14

Caption for Movie S1. LCE Hinge Duty Cycle Testing. A compilation of hinge duty cycle testing is presented. Three duty cycles are shown, 1%, 2%, and 3%. The hinge is shown actuating but unloaded and under a 2 g load.

Caption for Movie S2. Self-Folding LCE Crane and Miura Sheet Soft Robotic Actuation. The self-folding crane is shown folding from the fully flat configuration to the fully folded configuration and flapping its wings independently. The Miura sheet is also shown transitioning between its reconfigurable states. Both demonstrations are accompanied by thermal imaging and live power utilization and heating diagrams. Animated version of Figure 6 and Figure 7.

Caption for Data S1. Princeton Data Commons Repository All datasets used in this publication have been uploaded to a Princeton Commons data repository (`https://datacommons.princeton.edu/discovery/catalog/doi-10-34770-q55n-0m58`) and are available for further use. A readme.md and readme.txt file with descriptions of each file are included.